NASA Technical Memorandum 78522

Flight Research Capabilities of the NASA/Army Rotor Systems Research Aircraft

Samuel White, Jr. and Gregory W. Condon

September 1978

National Aeronautics and
Space Administration

NASA Technical Memorandum 78522

Flight Research Capabilities of the NASA/Army Rotor Systems Research Aircraft

Samuel White, Jr.
Gregory W. Condon, Ames Research Center, Moffett Field, California

NASA
National Aeronautics and
Space Administration

Ames Research Center
Moffett Field, California 94035

FLIGHT RESEARCH CAPABILITIES OF THE NASA/ARMY ROTOR SYSTEMS RESEARCH AIRCRAFT

Samuel White, Jr. and Gregory W. Condon*
Ames Research Center, NASA
Moffett Field, California 94035, U.S.A.

INTRODUCTION

The Rotor Systems Research Aircraft (RSRA) (Fig. 1) is being developed jointly by the National Aeronautics and Space Administration (NASA) and the United States Army under a contract to Sikorsky Aircraft Division, United Technologies Corporation. Two RSRA vehicles will be developed and delivered under the contract to provide the U.S. Government with a national facility capable of in-flight investigation and verification of promising new rotor concepts and supporting technology.

The two RSRA are currently undergoing developmental flight testing; one is scheduled to be delivered to the Ames Research Center in the fall of 1978 and the other in the spring of 1979. The research capabilities that will have been developed and demonstrated at the time of delivery of the first RSRA, which is configured as a helicopter, have been defined from flight test data that are available as of this writing. The research capabilities that will have been developed and demonstrated at the time of delivery of the second RSRA, which is configured as a compound helicopter, can be partially inferred from flight test and simulation data that are available as of this writing. This paper addresses these data with regard to expected research capabilities and limitations at the time of delivery and, where possible, compares these capabilities to the original design requirements.

BACKGROUND

The evolution of the RSRA concept and the projected research capabilities and uses of these vehicles have been presented in a number of previous papers (Refs. 1-4). The objective of the RSRA development program is to provide a versatile rotor research facility capable of precise measurement and control of rotor forces and of aircraft maneuvering flight parameters over a broad range of operating conditions. A related objective is to provide adaptability for installation of a variety of new rotors, thereby permitting development of promising advanced rotor concepts without the costly and time-consuming process of developing new or modified vehicles.

DESCRIPTION

One RSRA is configured as a helicopter and the other as a compound helicopter. In the helicopter configuration (Fig. 2), the RSRA has a design gross weight of 18,400 pounds. It is powered by the Sikorsky S-61 rotor and drive system, which consists of two T58-GE-5

*Formerly Structures Laboratory, U.S. Army Research and Technology Laboratories (AVRADCOM), Langley Research Center, Hampton, Virginia 23665, U.S.A.

turboshaft engines driving the S-61 main transmission, the 62-foot diameter main rotor, tail takeoff drive shaft, intermediate gear box, tail gear box, and the 11-foot diameter tail rotor. The horizontal stabilizer is a "T" tail with a 13-1/4-foot span and an area of 35.4 square feet.

In the compound configuration (Fig. 3), the 8SRA has a design gross weight of 26,200 pounds. Wing and auxiliary thrust jet engines are added to the helicopter and the tail is changed. The tail change includes adding a 22-1/2-foot span lower horizontal stabilator (stabilizer-elevator), a rudder, and associated controls; and replacing the helicopter fixed stabilizer with a smaller 8-1/2-foot span stabilizer. The wing has a 45-foot span and includes both aileron and flap surfaces. The wing incidence is variable in flight from -9° to +15°. The two auxiliary jet engines are TF-34-GE-400A high-bypass-ratio turbofans with maximum rated static thrust (SLS) of 9,275 pounds each.

The main transmission and rotor are mounted to the airframe through a balance system. Two systems are available and both have been flight-tested: one is a conventional load-cell system (Fig. 4); the other is an active isolation and balance system (Fig. 5) that provides broadband vibration attenuation as well as rotor load measurement. A wing load-cell system provides wing lift, drag and pitching moment measurements (Fig. 6). The tail rotor and auxiliary engine load cell systems provide axial thrust measurements (Fig. 7).

An emergency escape system is provided for the crew (Fig. 8). When the full egress mode is actuated, an all-pyrotechnic system severs the main rotor blades, jettisons and fractures the canopies, and initiates the crew extraction system. Tractor rockets connected to torso harnesses extract crew members and initiate parachute deployment. An alternative "blades only" mode, which provides for jettisoning the blades in the event of rotor problems that threaten the aircraft, permits flight as a fixed-wing aircraft. The crew consists of a safety pilot (aircraft commander) in the right seat, an evaluation pilot (copilot) in the left seat, and an aft-facing flight engineer seated behind the evaluation pilot.

A relatively conventional hydromechanical flight control system is provided for the safety pilot (Fig. 9), except that variable phasing between rotary-wing and fixed-wing control surfaces is provided by control phasing units. The flight control system includes analog force feel and stability augmentation systems. A digital, fly-by-wire control system is provided for the evaluation pilot (Fig. 10).

FLIGHT CAPABILITIES AND LIMITATIONS

The 8SRA has been designed for use in flight investigations of advanced rotor concepts and improvements in analysis/design methodology. The investigations of analysis/design methodology will start with the S-61 rotor system: they require a flight envelope in the regions for which the methodology improvements are being developed, aircraft control and handling qualities that permit accurate control of test conditions, and accurate measurement of the rotor and vehicle states that provide data for correlation with the analysis/design methodology. In addition to the capabilities required for methodology investigations, advanced rotor systems investigations require structural capabilities and dynamic characteristics that will permit investigation of advanced rotors, both within and outside the flight envelope demonstrated for the S-61 rotor.

The RSRA requirements for flight research capability have been investigated during the contractor development program. In addition to having been flight tested in both helicopter configurations and in the full compound configuration, the RSRA has been flight tested in two configurations leading to the full compound configuration. The first configuration was that of a helicopter with the compound tail; the other was that of a compound helicopter without the wing (Fig. 11). The RSRA is currently being flown in the full compound configuration. Finally, the rotor will be removed and the RSRA will be flown as a fixed-wing aircraft.

In general, the capabilities of the RSRA are expected to be adequate to begin flight research operations. These capabilities will be presented as based on flight test data and comparisons with design limits or predicted results. Substantial analytical, wind-tunnel, and simulation efforts have been undertaken during the development of the RSRA in attempts to predict its flight characteristics, to evaluate those characteristics against required flight research capabilities, and to aid in resolving shortcomings in the design. Given the RSRA requirements for versatility, the resulting complexity of flight configurations, and the need to contain development costs, it has been necessary to make compromises in vehicle capabilities; these compromises will be addressed.

Helicopter Configurations

As noted, there are two helicopter configurations: one in which the transmission is mounted to the airframe by load cells and one in which the transmission is mounted by an active isolation balance system. This paper will discuss only the configuration with the load-cell system. The unique characteristics associated with the active isolation balance system are covered by another paper presented in this forum, Paper No. 18, entitled "The RSRA Active Isolation/Rotor Balance System" by J. Madden and W. Kuczynski.

Structures

The flight envelope for the RSRA in the helicopter configuration with the load-cell balance system was developed for a maximum takeoff gross weight of 19,800 pounds, a midcenter-of-gravity location (302 inches), and a maximum density altitude of 3,000 feet. The envelope for powered straight and level flight is shown in Figure 12, the normal operating rpm being 104%. As shown, the only components experiencing fatigue damage in straight and level flight are the push rod and the upper horizontal stabilizer attachment fitting. A value of 104% N_R was chosen as the normal operating rpm because, as the curve of pushrod vibratory load endurance limit exceedance shows, at this rpm the lowest stresses exist while maintaining an rpm range for variations during maneuvers. The power-off envelope is 94% to 115% N_R below 135 KCAS. All stresses were less in power-off flight than in powered straight and level flight.

Figure 13 shows pushrod vibratory load versus airspeed, the load exceeding the endurance limit (END). The steep gradient of the curve coupled with a do-not-exceed limit (DNE) of 2,400 pounds dictated the maximum forward speed of 153 knots. Pushrod load is the limiting load in the rotating controls and could be expected to be the limiting parameter for flight testing of different blades on the existing RSRA hub. As shown in Figure 14, the right lateral stationary star vibratory load is just below the endurance limit at 153 KCAS at normal operating rpm.

This parameter is the critical component in the nonrotating controls and could be expected to be the limiting parameter for investigation of different rotors that could be adapted to the RSRA rotor shaft.

The vibratory stress on the upper horizontal stabilizer attachment fitting, as was shown in Figure 12, exceeds the endurance limit in straight and level flight within the demonstrated envelope (Fig. 15). Although this attachment fitting is redundant and readily inspectable, a modification to correct the exceedance is currently under consideration. Figure 15 also shows the next highest reading vibratory airframe stress, a tail pylon gage, which is well below the endurance limit. The steady stresses in the airframe are quite low. This is as expected since the airframe was designed to fly a more powerful rotor (called "Super Rotor") and to withstand 4 g at 300 knots as a compound.

The limiting tail rotor parameter, blade vibratory stress, is shown versus airspeed in Figure 16. The tail rotor is not a limiting factor within the level flight envelope, and should not be a limiting factor for main rotors which do not exceed S-61 power requirements.

The forward flight maneuvering envelope is shown in Figure 17. The outer envelope is the fuselage structural design envelope; the inner envelope is the RSRA demonstrated envelope. The trends of endurance limit exceedances for the pushrod and upper horizontal stabilizer attachment fitting, both of which exceed the endurance limit in straight and level flight, are shown. In addition to these parameters, other parameters also exceed endurance limits.

Figure 18 presents the design envelope of sideslip versus airspeed for the helicopter fuselage and the envelope attained during flight testing. As shown, the only component experiencing fatigue damage is the tail rotor spindle. However, at point A, the pitch beam load, thrust load cell load, and blade total stress are close to the endurance limit.

In hover, all parameters are well below their endurance level. The envelope for sideward flight is 20 knots right and 30 knots left with the rudder removed. However, the original configuration for the helicopter included the rudder installed. As shown in Figure 19, with the rudder installed and the aircraft at a gross weight of 17,236 pounds, the tail rotor pitch beam load was approximately at the endurance limit. The vertical tail/rudder combination was providing very high blockage (57% of the tail rotor disc shadowed by the tail/rudder) resulting in high control loads and, as will be subsequently discussed, low control power. Removal of the rudder reduced the blockage (to 36%) and, as shown, dramatically reduced the pitch beam load.

The hovering turn envelope for the RSRA, which is 20 seconds for a 360° turn, may result in fatigue damage to the tail rotor controls, blades, and thrust load cell.

Each endurance limit exceedance requires calculation of fatigue damage and continuous tracking of cumulative fatigue damage. Fatigue life calculations, using the RSRA repeated load design spectrum and anticipated usage, indicate that the fatigue life of the most critical component in fatigue exceeds the expected service life of the aircraft by an order of magnitude, and that component replacement, because of fatigue life problems, will be unlikely. To ensure structural integrity for fatigue, however, cumulative fatigue damage will continue to be

tracked on a flight-by-flight basis throughout the life of the aircraft. If subsequent data, such as high-speed compound flight, indicate a trend in cumulative damage that will require component replacement, such replacements will be scheduled and provisioned. Fatigue life, therefore, is not expected to be a limitation on the use of the RSRA.

Handling Qualities

Level flight controllability data, presented in Figure 20, show no unacceptable characteristics. As expected, significant changes did not result from changing normal operating rpm from 100% to 104% for the structural considerations previously mentioned. The test results show that the tail rotor impressed pitch agrees well with predictions throughout the airspeed range, and that longitudinal control and pitch attitude agree well with predictions at low airspeeds but not at high airspeeds. The reason for the poor correlation is unknown but will be investigated during research operations by NASA and the Army. This unexplained disagreement coupled with the proximity of the control stop (15% of travel from neutral) at 153 KCAS requires caution for envelope development at aft center of gravity locations. However, the horizontal stabilizer is ground-adjustable and adjustment will be used as a means to alleviate this problem.

As shown in Figure 21, the longitudinal static stability is marginally positive at 70 KCAS, which is the airspeed at which the static stability is predicted to be the lowest. As shown in Figure 22, the helicopter configuration exhibits positive lateral directional static stability.

The dynamic response of the RSRA helicopter is well damped for all axes in forward flight as shown for yaw in Figure 23. There is positive dihedral as evidenced in the figure also.

Pitch and roll control sensitivity and damping in a hover are shown in Figures 24 and 25. The low-pitch sensitivity coupled with the relatively higher roll sensitivity is due to large differences in inertia (96,000 slug-ft^2 in pitch versus 8,800 slug-ft^2 in roll). This control disharmony manifests itself in terms of a PIO tendency (Fig. 26). This disharmony problem can be alleviated by reducing the roll sensitivity through use of the control phasing unit. Reduction of roll sensitivity will be undertaken by NASA and the Army during initial government research operations. The yaw control sensitivity versus damping is shown in Figure 27. The extremely low yaw control sensitivity results from the high yaw inertia and makes hovering in gusty air difficult.

The requirements for tail rotor control for sideward flight are shown in Figure 28. Note that with the rudder installed, there is a significant loss in tail rotor control power. Removal of the rudder provides adequate trim control throughout the sideward flight envelope; however, the low control sensitivity necessitates a larger than normal control margin. As a result, maneuvering flight in a hover is not recommended in windy or gusty conditions and a limit of 20 seconds for a 360° turn is imposed.

Dynamics

Cockpit vibration data at N/rev for both pilot stations are shown in Figure 29 versus airspeed and are the result of one tuning change to

the bifilar absorbers. Only minor variations in vibration levels occur over the rotor rpm range. The vibration levels experienced by the T-58 engines and tail rotor drive system were all within allowable limits.

Helicopter With Compound Tail Configuration

The helicopter with the compound tail was flown (1) in order to investigate the effect on pitch-axis handling qualities of rotor downwash on the compound tail, and (2) to validate the mathematical modeling of this phenomenon so as to provide confidence in the prediction of the minimum speed for the compound prior to first flight. As shown in Figure 30, the pitch attitude prediction was quite accurate (in contrast to the helicopter prediction which diverged at forward speeds); however, the longitudinal control differed from the predicted control at airspeeds below about 60 knots, showing a stick reversal. Consequently, 60 knots was set as the lower limit to which the predictions were considered valid for the compound.

Wingless Compound Configuration

The TF-34 fan jets were added to the helicopter with the compound tail in order to investigate power management and to validate the mathematical modeling of the jet engines effect on handling qualities at low speeds. As a result of these limited objectives, this configuration was flown well within the envelope of the helicopter configuration.

Structures

This configuration was flown at 23,500 pounds gross weight, midcenter-of-gravity location (302 inches), and normal operating rpm (104%). Figure 31 shows the helicopter structural design envelope, the helicopter flight test envelope, and the wingless compound flight test envelope, all with their associated gross weights. The critical main rotor parameter is not the pushrod load, as it is in the helicopter configuration, but rather the right lateral stationary star vibratory load, as shown in Figure 32.

In comparison to the helicopter configuration, the added gross weight (from 19,700 pounds to 23,500 pounds) due to TF-34 installation causes a decrease of about 40 knots in the speed at which the star load increases dramatically. Therefore, a maximum level flight speed of about 115 knots could be expected for the compound with a wing incidence that would result in a rotor lift of 23,500 pounds and a rotor propulsive force sufficient to overcome a drag slightly less than the helicopter fuselage drag (with TF-34 engines in idle, the TF-34/nacelle has a slight propulsive force). Reduction of the main rotor torque by 20% at 90 KCAS results in a significant reduction in star load (2,600 to 900 pounds). Using TF-34 thrust to increase forward speed from this trim condition results in an increase of about 20 knots in the speed at which the dramatic load increase occurs, thereby demonstrating, as one would expect, that reduction in torque and the use of TF-34 thrust will allow increased forward speed even while maintaining high lift.

The critical tail rotor parameter, as was the case in the helicopter, is blade vibratory stress (Fig. 33). The basic trends in the data with application of TF-34 thrust are similar to the trends in right lateral stationary star load.

As regards fuselage stresses in this configuration, the tail pylon vibratory stress, as shown in Figure 34, remains consistent with helicopter data. Also, as shown in Figure 34, the upper horizontal stabilizer attachment vibratory stresses are reduced relative to the helicopter. This is due to the large upper stabilizer being replaced by a smaller one for the compound configurations. The fuselage stresses obviously pose no problems for this configuration and flight envelope.

The envelope for sideslip versus airspeed is shown in Figure 35 and was investigated to understand tail rotor loads in the event of one TF-34 being inoperative. The stresses were all less than endurance values within the envelope.

Handling Qualities

The primary handling qualities concern was the effect of the TF-34 engines on handling qualities in the pitch axis and verification of the accuracy of the predictions prior to compound flight. Figure 36 shows a comparison of predicted and actual pitch attitude and longitudinal control versus airspeed for TF-34s at idle and for main rotor torque at 20% less than the value required at 90 KCAS with TF-34s in idle. The correlation is quite good and resulted in high confidence in the predictions for compound handling qualities. The takeoff speed for this configuration was chosen a priori at 80 knots. Note that the longitudinal control reversal occurs at 80 knots versus 60 knots for the helicopter with the compound tail.

Dynamics

Figure 37 shows copilot vertical acceleration at N/rev and, although within acceptable limits, the levels are higher than in the helicopter configuration. Reduction in main rotor torque and use of TF-34 thrust to increase speed result in reductions in main rotor vibratory forcing functions and, as expected, reductions in cockpit vibrations.

Compound Configuration

The flight envelope development program for the compound configuration is currently ongoing.

Structures

The vehicle is being flown at 26,200 pounds takeoff gross weight, midcenter-of-gravity position (302 inches), and a maximum density altitude of 3,000 feet. As of this writing only very limited flight investigations have been conducted. The forward flight maneuvering envelope is shown in Figure 38. The outer envelope is the structural design envelope, the middle envelope is the planned demonstration envelope, and the inner envelope is the accomplished envelope as of this writing.

Figure 39 shows right lateral stationary star vibratory load versus airspeed for the helicopter, wingless compound, and compound configurations. This parameter, not pushrod load, is the critical parameter for both the full compound and the wingless compound configurations. As can be seen by examining the cases for the TF-34 engines at ground idle, the addition of the wing to the wingless compound

increases the speed of the knee of the curve by about 15 knots. This is due to the reduced rotor lift which, over the speed range of 75 to 116 knots, is predicted to vary from 19,700 pounds to 17,000 pounds. Because the increased fuselage drag requires a much higher propulsive force, the compound data do not agree with the helicopter data even though the rotor lifts are approximately equal. Setting the main rotor torque to equal the torque at 80 knots with the TF-34 engines in idle and using the TF-34 engines to increase speed, results in reduced load as anticipated.

Figure 40 shows tail rotor blade vibratory stress versus airspeed for the helicopter, wingless compound, and compound configurations. The same trends as discussed for the right lateral stationary star appear.

Figure 41 shows the vibratory stress of the upper horizontal stabilizer attachment fitting and tail pylon vibratory stress, the two fuselage master indicators, versus airspeed. The stress levels fall among the wingless compound data and pose no limits within the flight speeds investigated.

Handling Qualities

The data for trim longitudinal control in level flight with TF-34 engines at idle are shown in Figure 42 along with the predicted trim. As can be seen, there is excellent correlation. The stick reversal again is predicted to occur at about 80 knots. Figure 43 shows the trim characteristics with rate of climb at 80 KCAS; predictions correlate well with the limited data available. The lift-off speed was chosen as 80 knots because of degraded handling qualities below this speed and because of attitude considerations. The takeoff technique is to set the TF-34 engines to 50% N_F with the brakes applied; to release the brakes and accelerate to 80 KCAS with the TF-34 engines at 50% N_F; to roll the throttle back to the idle detent (24% N_F); and to lift off and climb out using collective. This technique allows a short takeoff roll; permits a nose down rotation at lift-off since the trim attitude in climbout at 500 feet per minute is approximately 1.5° versus a ground attitude of 2.5°; lifts the tail wheel first; and facilitates maintaining 80 knots in transition to the climbout. Lift off at 50% N_F is not desirable since this would require a large nose-up attitude change (from 2.5° ground attitude to 7.5° climb attitude) to transition to the climb condition.

Dynamics

The co-pilot vertical acceleration at N/rev is shown in Figure 44 for the helicopter, wingless compound, and compound configurations. Again as expected, the reduction in rotor lift of the compound with respect to the wingless compound results in lower cockpit vibrations because the rotor forcing functions are reduced.

Load Cell Systems

As discussed under "Background" and "Description," the basic objective of the RSRA, to provide precise measurement of flight loads, is provided by the on-board measurement system. During the contractor's development flight test program, load-cell data have been used almost exclusively for structural substantiation of airframe components. The load-cell balances have not been calibrated as a system to determine

influence coefficients or system accuracy. System calibrations are scheduled as the first task of the Government's research flight operations phase. Until the system has been calibrated, precise comparisons cannot be made between measured loads and theoretical values or values determined by other independent measurements. Simplified tests of reasonableness, however, can provide an indication of anticipated capability and utilization of calibrated flight data. The examples that follow are intended to illustrate potential uses of load-cell data in research operations. The first illustration, Figure 45, shows measured values of rotor and wing lift versus airspeed for unaccelerated forward flight of the compound configuration with a wing incidence angle of +10°. The difference between these net lift forces with the lift body axis component of gross weight is a measure of down-load on the fuselage/empennage. In the uncalibrated example, the difference also includes errors due to excluding the influence of other load cells, redundant load paths, vertical load factor, and systematic or random errors.

Similarly, Figure 46 compares measured forces in the drag/propulsive force body axis. In this example the net propulsive forces are summed and the drag of the fuselage/empennage inferred. This inferred value of drag is compared with wind-tunnel data. The wind-tunnel data have been corrected to body-axis components and adjusted to remove wing and auxiliary engine contributions, to provide a direct comparison with flight data. As in the preceding example, use of uncalibrated data, as well as the imprecision in applying correction factors to wind-tunnel data, tend to introduce error. A further major factor is the absence of tail rotor drag in the wind tunnel data.

Figure 47 compares yawing moments measured at the main rotor torque load cells with tail rotor antitorque and vertical stabilizer yawing moments. The latter were calculated from wind-tunnel data using yaw angles measured in flight. Again, apparent error is attributed primarily to use of uncalibrated data and the influence of other load cells or redundant links.

After calibration of the on-board measurement system, analyses similar to the examples presented will be conducted for the forces and moments in all three axes of the rotor force measurement system. The questions raised by the "errors" in the examples provide intriguing and challenging areas of research made possible by the availability of the RSRA.

CONCLUDING REMARKS

As we approach the conclusion of the RSRA development program and the beginning of research flight operations, our assessment of the expected research capabilities of the RSRA is favorable. The structural limitations should not significantly constrain the flight envelope for research operations; the handling qualities, although not optimum, are within the parameters originally predicted; and there are no fundamental dynamics problems. Although the accuracy of the force and moment measurement systems has not yet been quantified by calibration, it is expected to be acceptable after calibration. Some of the questions and gaps in information that have been raised during our assessment of RSRA capabilities suggest areas for early research projects.

influence coefficients or system accuracy. System calibrations are scheduled as the first task of the Government's research flight operations phase. Until the system has been calibrated, precise comparisons cannot be made between measured loads and theoretical values or values determined by other independent measurements. Simplified tests of reasonableness, however, can provide an indication of anticipated capability and utilization of calibrated flight data. The examples that follow are intended to illustrate potential uses of load-cell data in research operations. The first illustration, Figure 45, shows measured values of rotor and wing lift versus airspeed for unaccelerated forward flight of the compound configuration with a wing incidence angle of +10°. The difference between these net lift forces with the lift body axis component of gross weight is a measure of down-load on the fuselage/empennage. In the uncalibrated example, the difference also includes errors due to excluding the influence of other load cells, redundant load paths, vertical load factor, and systematic or random errors.

Similarly, Figure 46 compares measured forces in the drag/propulsive force body axis. In this example the net propulsive forces are summed and the drag of the fuselage/empennage inferred. This inferred value of drag is compared with wind-tunnel data. The wind-tunnel data have been corrected to body-axis components and adjusted to remove wing and auxiliary engine contributions, to provide a direct comparison with flight data. As in the preceding example, use of uncalibrated data, as well as the imprecision in applying correction factors to wind-tunnel data, tend to introduce error. A further major factor is the absence of tail rotor drag in the wind tunnel data.

Figure 47 compares yawing moments measured at the main rotor torque load cells with tail rotor antitorque and vertical stabilizer yawing moments. The latter were calculated from wind-tunnel data using yaw angles measured in flight. Again, apparent error is attributed primarily to use of uncalibrated data and the influence of other load cells or redundant links.

After calibration of the on-board measurement system, analyses similar to the examples presented will be conducted for the forces and moments in all three axes of the rotor force measurement system. The questions raised by the "errors" in the examples provide intriguing and challenging areas of research made possible by the availability of the RSRA.

CONCLUDING REMARKS

As we approach the conclusion of the RSRA development program and the beginning of research flight operations, our assessment of the expected research capabilities of the RSRA is favorable. The structural limitations should not significantly constrain the flight envelope for research operations; the handling qualities, although not optimum, are within the parameters originally predicted; and there are no fundamental dynamics problems. Although the accuracy of the force and moment measurement systems has not yet been quantified by calibration, it is expected to be acceptable after calibration. Some of the questions and gaps in information that have been raised during our assessment of RSRA capabilities suggest areas for early research projects.

REFERENCES

1) Robert J. Huston et al.: The Rotor Systems Research Aircraft – A New Step in the Technology and Rotor System Verification Cycle. Presented at the AGARD Flight Mechanics Panel Symposium on "Rotorcraft Design," Ames Research Center, Moffett Field, California, May 16-19, 1977.

2) Gregory W. Condon, Rotor Systems Research Aircraft (RSRA) Requirements for, and Contributions to, Rotorcraft State Estimation and Parameter Identification. Presented at the AGARD Flight Mechanics Panel Specialists Meeting on "Methods for Aircraft State and Parameter Identification," Hampton, Virginia, November 5-8, 1974.

3) Robert Letchworth and Gregory W. Condon, Rotor Systems Research Aircraft (RSRA), Presented at the AGARD Flight Mechanics Panel Symposium, Valloire, France, June 9-12, 1975.

4) Frederick L. Moore and John J. Occhiato, The Basic Flying Characteristics of the Rotor Systems Research Aircraft, Presented at the 33rd Annual National Forum of the American Helicopter Society, Washington, D.C., May 1977.

Fig. 1 Rotor Systems Research Aircraft.

Fig. 2 RSRA helicopter configuration.

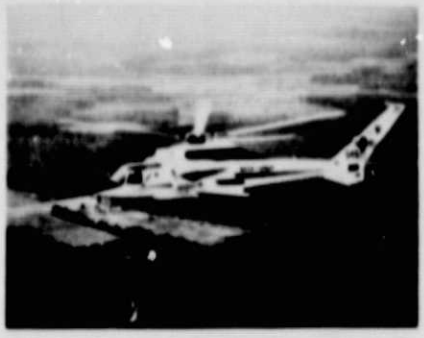

Fig. 3 RSRA compound configuration.

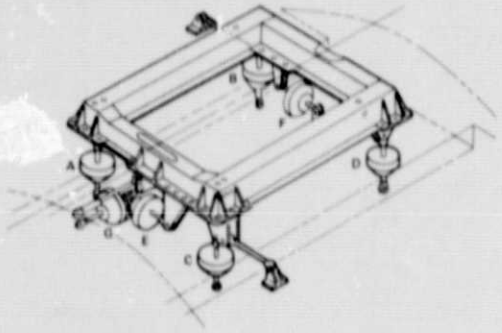

Fig. 4 Main rotor load measurement system.

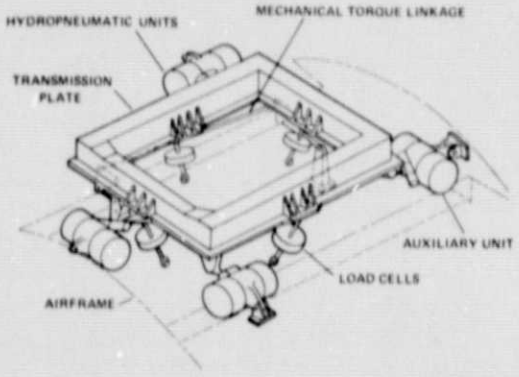

Fig. 5 Active isolation/balance system configuration.

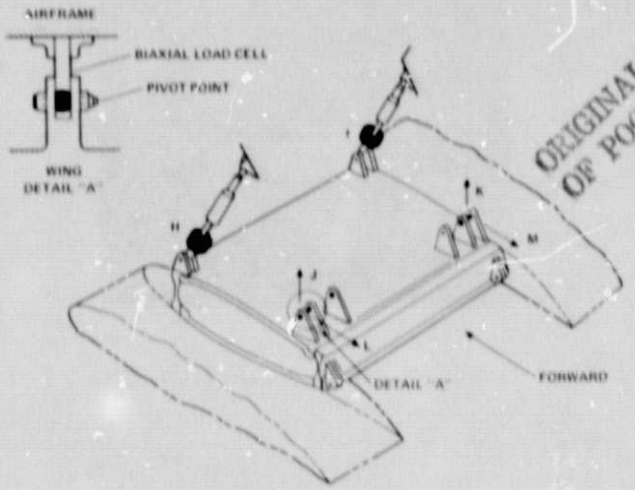

Fig. 6 Wing load measurement system configuration.

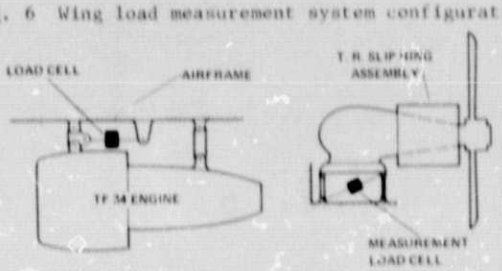

Fig. 7 Auxiliary propulsion and tail rotor thrust measurement systems configurations.

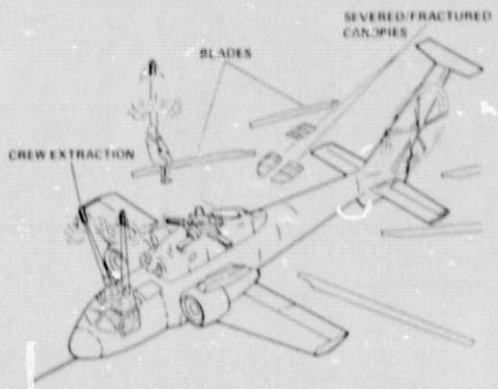

Fig. 8 Crew escape system.

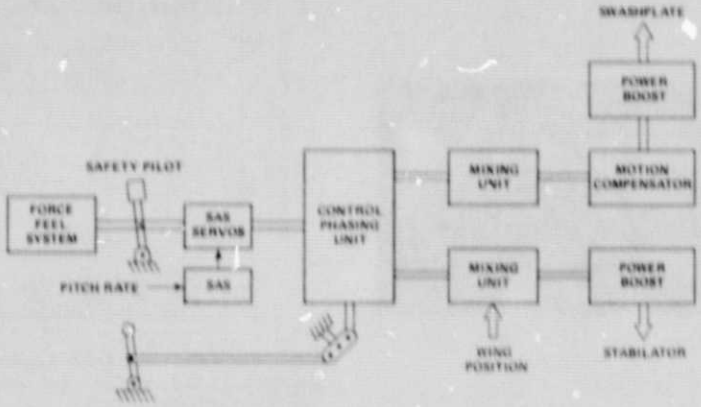

Fig. 9 Primary flight control system.

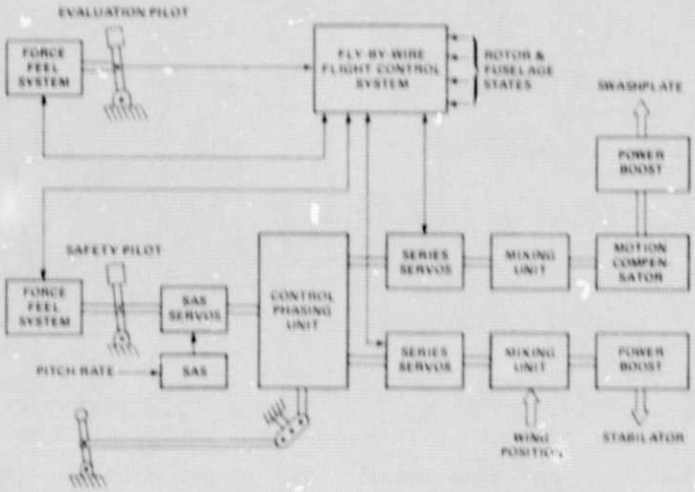

Fig. 10 Fly-by-wire flight control system.

Fig. 11 RSRA wingless compound configuration.

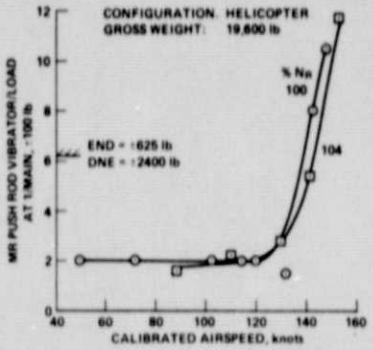

Fig. 13 Critical main rotor rotating controls load for the helicopter configuration.

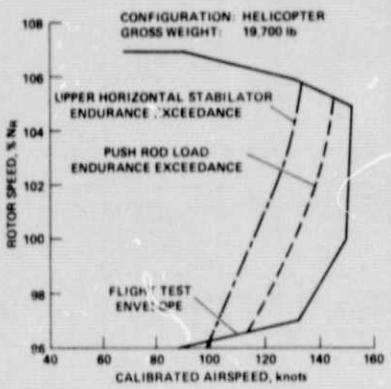

Fig. 12 Helicopter power-on envelope in level flight.

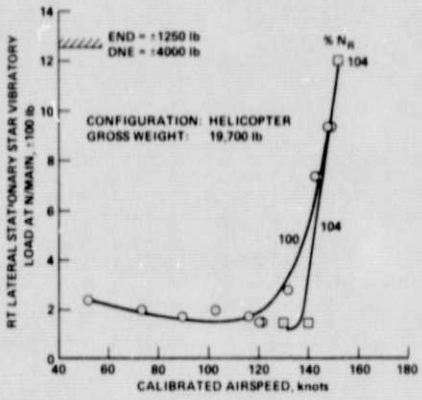

Fig. 14 Critical main rotor stationary controls load for the helicopter configuration.

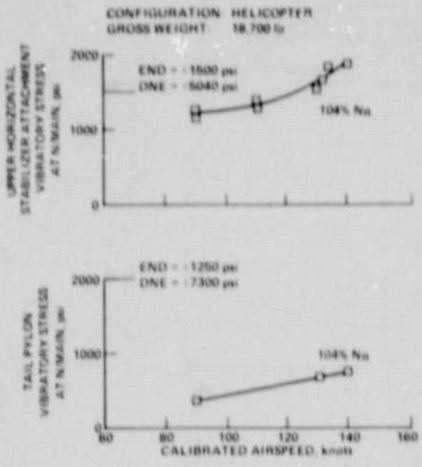

Fig. 15 Critical fuselage stresses for the helicopter configuration.

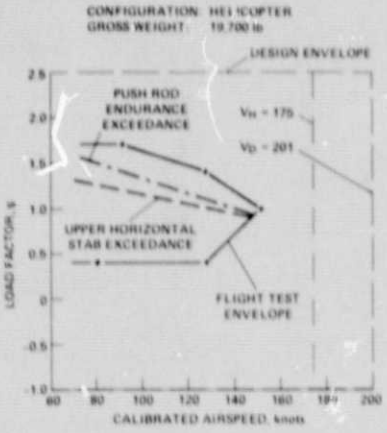

Fig. 17 Helicopter forward flight maneuvering envelope.

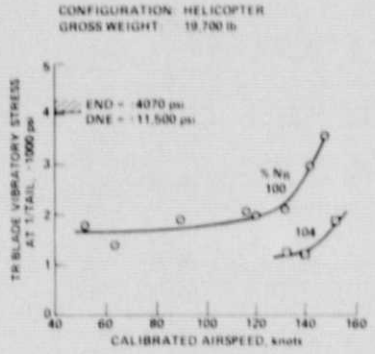

Fig. 16 Critical tail rotor load for the helicopter configuration.

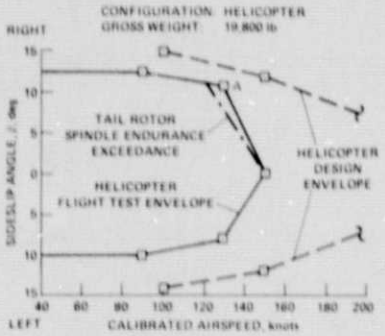

Fig. 18 Helicopter sideslip envelope.

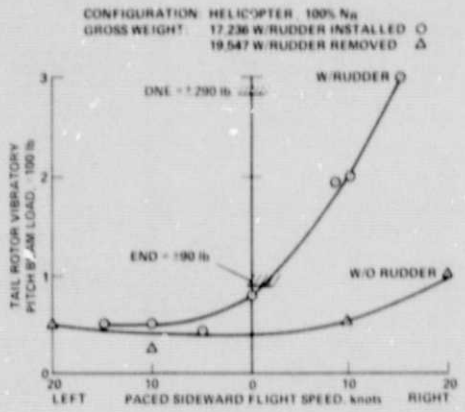

Fig. 19 Effect of rudder removal on tail rotor loads for helicopter in sideward flight.

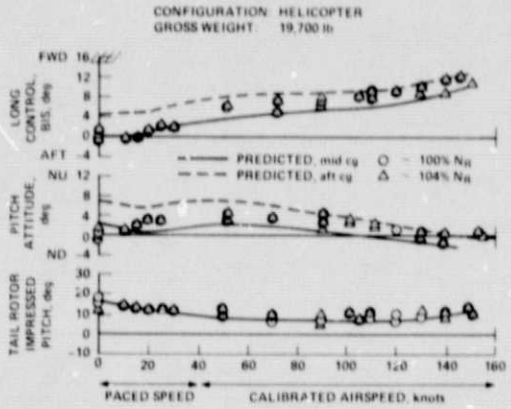

Fig. 20 Comparison of predicted and actual trim for the helicopter configuration.

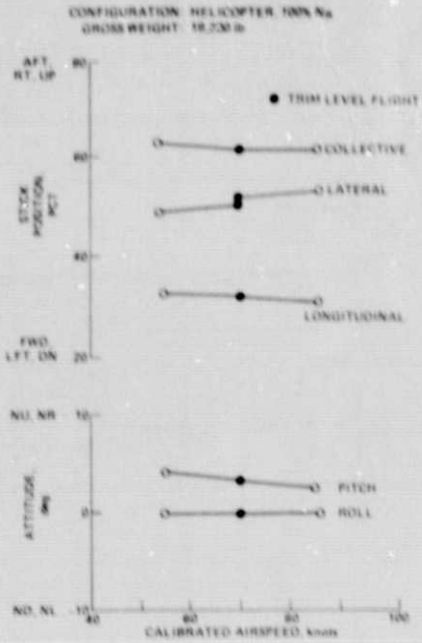

Fig. 21 Longitudinal static stability in the helicopter configuration.

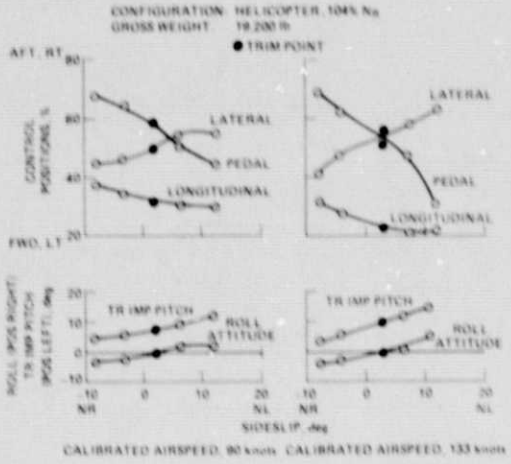

Fig. 22 Lateral directional static stability in the helicopter configuration.

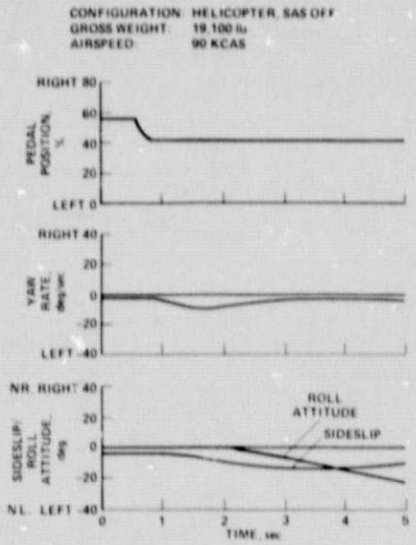

Fig. 23 Helicopter response to pedal step input in forward flight.

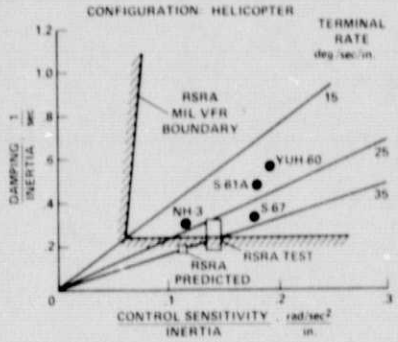

Fig. 24 Helicopter pitch control sensitivity/damping in a hover.

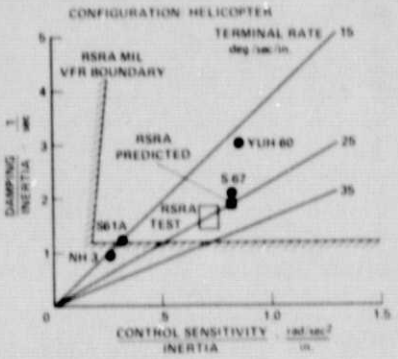

Fig. 25 Helicopter roll control sensitivity/damping in a hover.

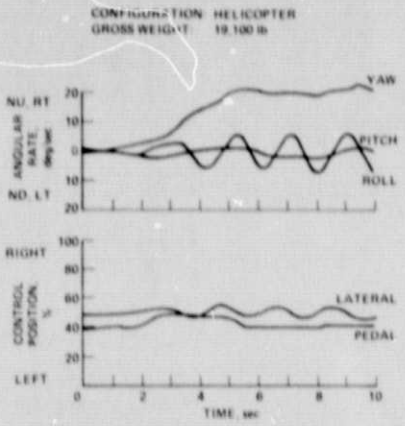

Fig. 26 Helicopter right hover turn.

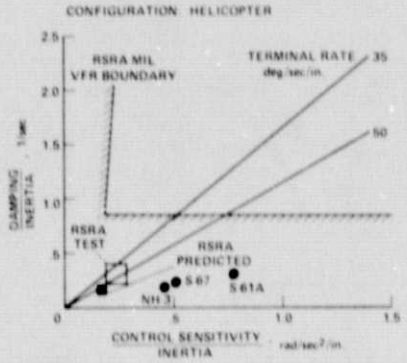

Fig. 27 Helicopter yaw control sensitivity/damping in a hover.

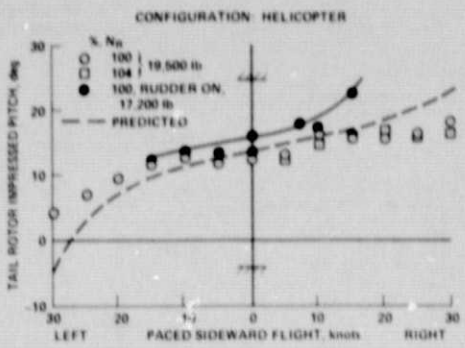

Fig. 28 Effect of rudder removal on tail rotor control for helicopter in sideward flight.

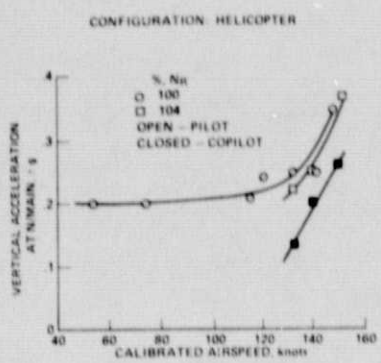

Fig. 29 Cockpit vibrations for helicopter configuration.

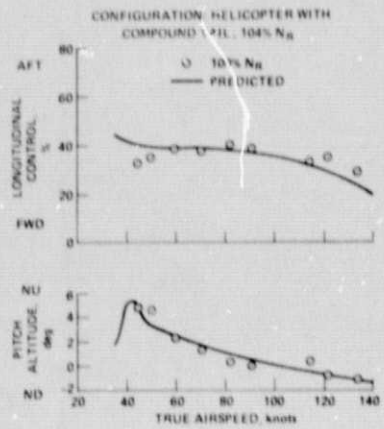

Fig. 30 Comparison of predicted and actual longitudinal trim for the helicopter with compound tail configuration.

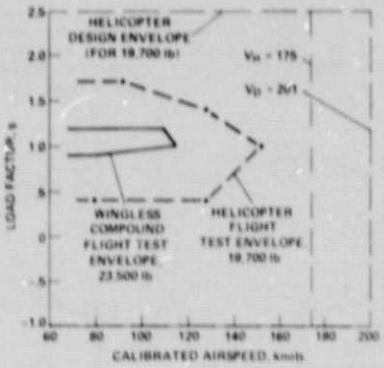

Fig. 31 Forward flight maneuvering envelope for the wingless compound configuration.

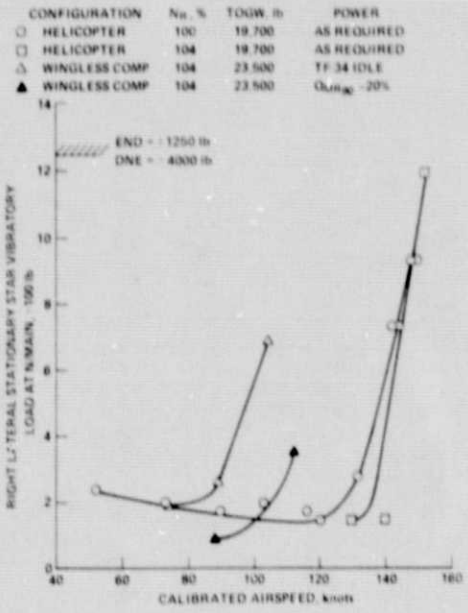

Fig. 32 Critical main rotor load for the wingless compound.

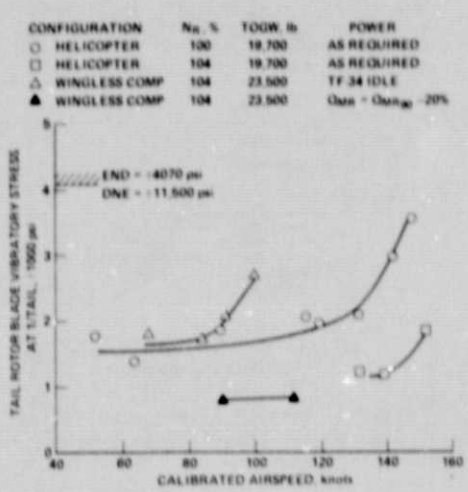

Fig. 33 Critical tail rotor load for the wingless compound.

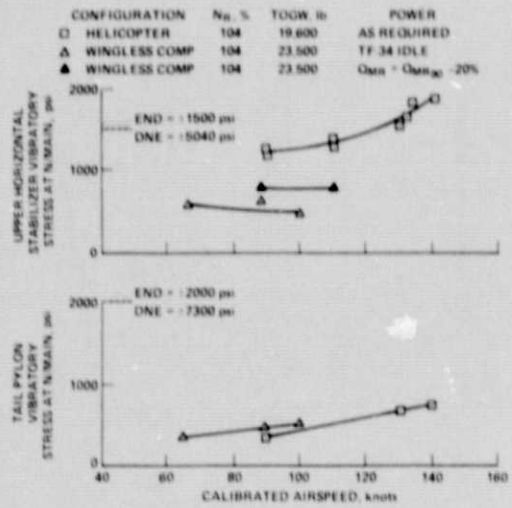

Fig. 34 Critical fuselage stresses for wingless compound.

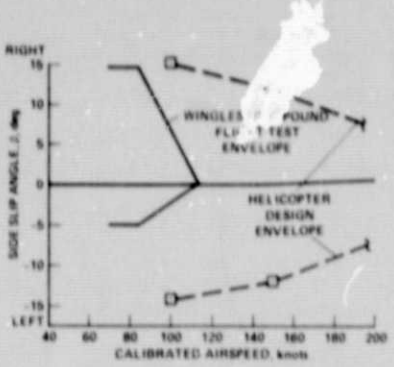

Fig. 35 Sideslip envelope for wingless compound.

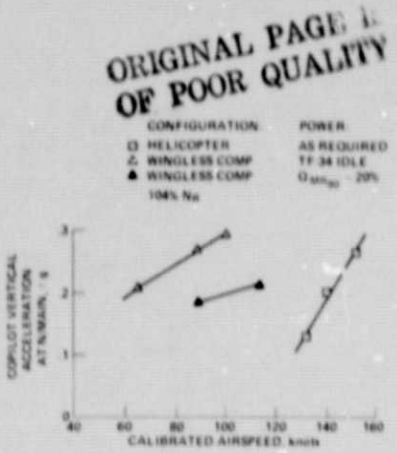

Fig. 37 Cockpit vibrations for wingless compound configuration.

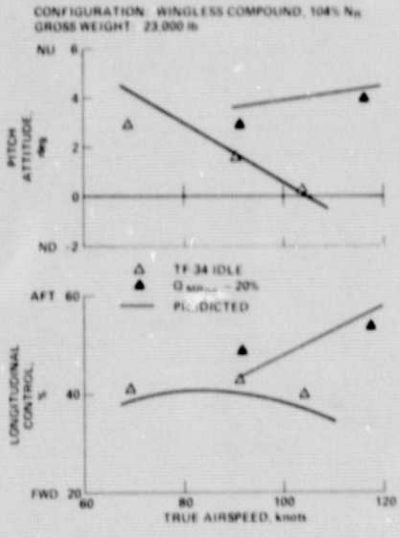

Fig. 36 Comparison of predicted and actual longitudinal trim for the wingless compound configuration.

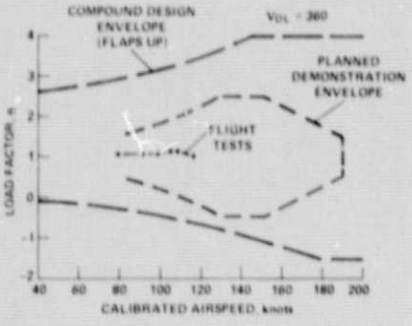

Fig. 38 Maneuvering envelope for compound.

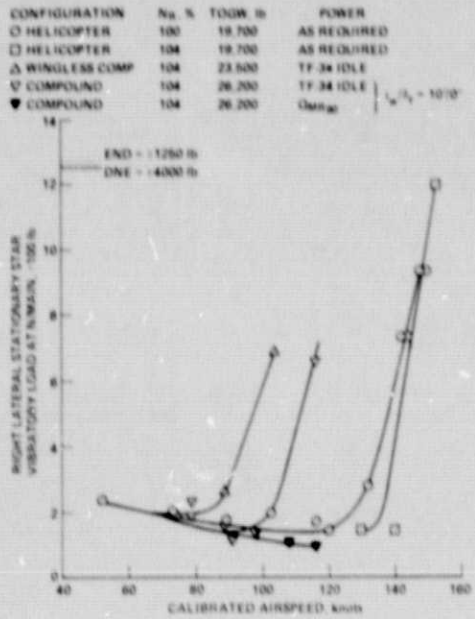

Fig. 39 Critical main rotor load for the compound configuration.

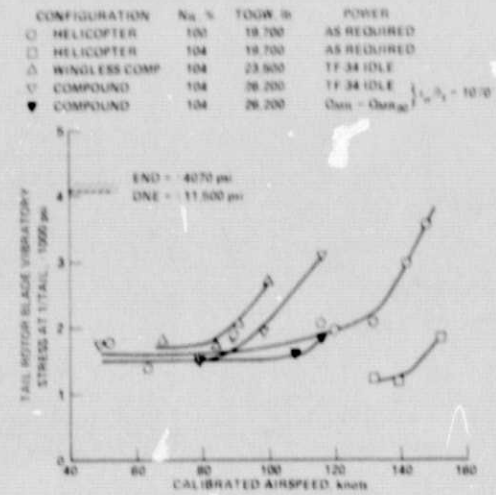

Fig. 40 Critical tail rotor load for the compound configuration

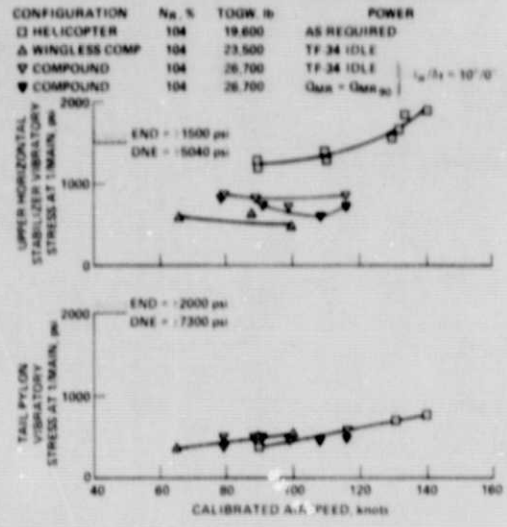

Fig. 41 Critical fuselage stresses for the compound configuration.

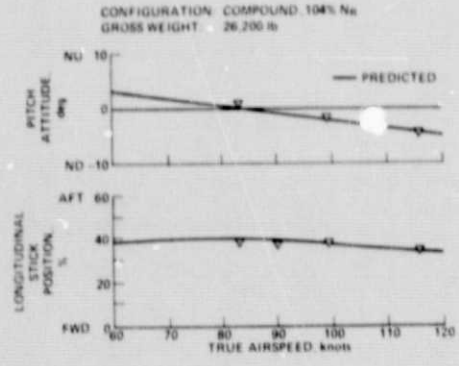

Fig. 42 Comparison of predicted and actual longitudinal trim for the compound configuration.

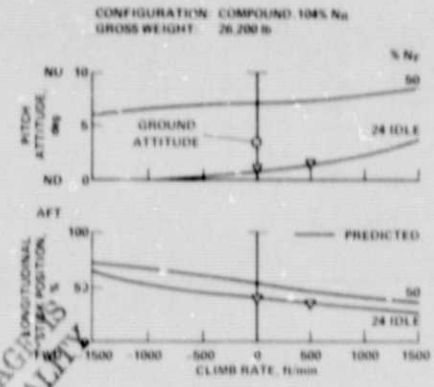

Fig. 43 Comparison of predicted and actual longitudinal trim in a climb for the compound configuration.

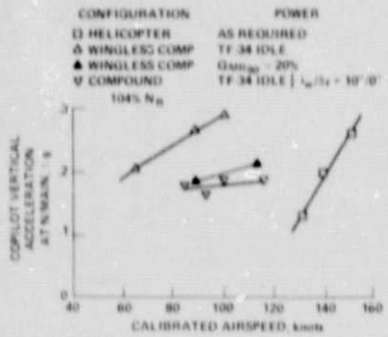

Fig. 44 Cockpit vibrations for compound configuration.

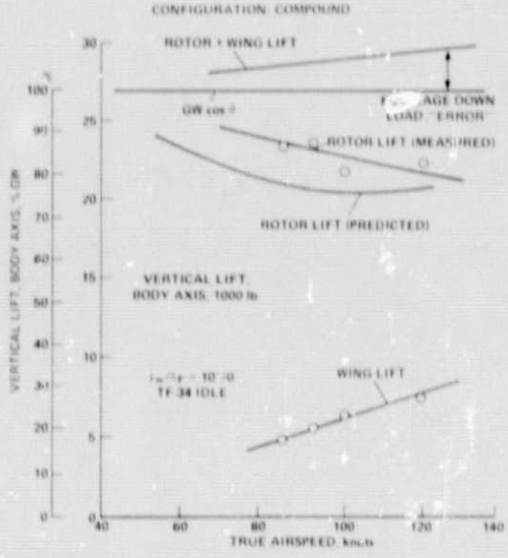

Fig. 45 Compound flight loads in vertical body axis.

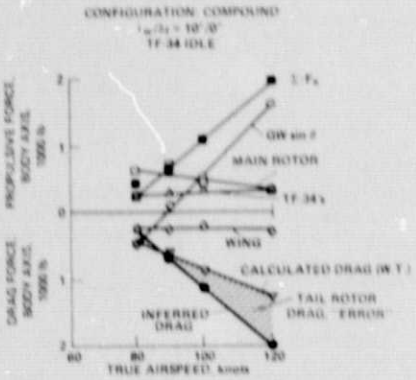

Fig. 46 Compound flight loads in longitudinal body axis.

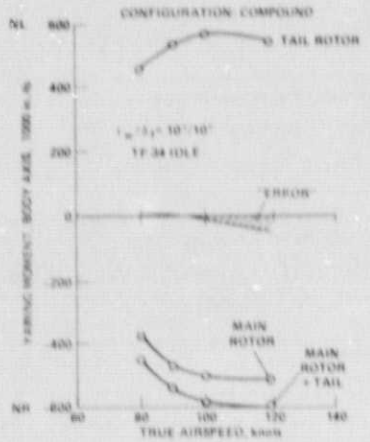

Fig. 47 Compound flight yawing moments.